Experimental and numerical study for direct powder bed selective laser processing (sintering/melting) of silicon carbide ceramic

Alejandro Montón, Mohammed Abdelmoula, Gökhan Küçüktürk, Francis Maury, David Grossin, Marc Ferrato

Materials Research Express

PAPER

Experimental and numerical study for direct powder bed selective laser processing (sintering/melting) of silicon carbide ceramic

Alejandro Montón[1], Mohammed Abdelmoula[2], Gökhan Küçüktürk[2], Francis Maury[1], David Grossin[1] and Marc Ferrato[3]

[1] CIRIMAT, Université de Toulouse, CNRS, France
[2] Department of Mechanical Engineering, Gazi University, Ankara 06500, Turkey
[3] Mersen Boostec, Zone Industrielle Bazet ouest, Bazet 65460, France

E mail: david.grossin@ensiacet.fr

OPEN ACCESS

RECEIVED
12 March 2021

REVISED
7 April 2021

ACCEPTED FOR PUBLICATION
12 April 2021

PUBLISHED
21 April 2021

Keywords: selective laser sintering, SiC, simulation, CFD, sintering, decomposition, additive manufacturing

Abstract

The study was carried out to investigate the manufacturing possibility of Silicon Carbide (SiC) by direct Powder Bed Selective Laser Processing (PBSLP) experimentally and numerically. The experimental study was carried out by means of PBSLP while the numerical study was accomplished by developing a CFD model. The CFD model simulates accurately realistic conditions of the PBSLP process. A user-defined code, that describes the process parameters such as laser power, scanning speed, scanning strategies, and hatching distance has been developed and compiled to ANSYS FLUENT 2020 R1. Also, the model was validated with the available published data from the literature. The model was used to deeply analyse and support the results obtained through the experimental runs. Different values of laser power and scanning speeds with scanning strategy in the form of a continuous linear pattern and rotated by 90 degrees between layers were studied. The laser power is ranging from 52W to 235 W while the scanning speed is ranging from 300 to 3900 mm s ^{1}. The results showed that the direct PBSLP of SiC is possible with the optimization of the process parameters. Layer thickness and hatching distance are the most important parameters that needed to be optimized. Also, the laser power and scanning speed needed to be adjusted so that the scanning temperature was between the sintering and the decomposition limits. The good agreement between experimental and simulation results proved the power and ability of the developed CFD model to be a useful tool to analyse and optimize future experimental data.

Nomenclatures

C_p	Specific heat (J kg ^{1}K ^{1})
T	Temperature (K)
k	Thermal conductivity (W m ^{1} K ^{1})
S_h	Laser heat source (Wm ^{3})
t	Time (s)
A	Material absorptivity
I_o	Laser intensity (Wm ^{2})
α	Absorption coefficient (m ^{1})
v_x	Laser velocity in x direction (ms ^{1})
v_y	Laser velocity in y direction (ms ^{1})
P	Pressure (Pa)
ω	Laser characteristic radius (m)

D_b	Laser spot diameter (m)
T_a	Initial temperature of powder layer (K)
T_s	Surroundings temperature (K)
h_{conv}	Heat convection coefficient ($Wm^{-2}K^{-1}$)

Greek Symbols

ρ	Density ($kg\,m^{-3}$)
ε	Radiation coefficient
σ	Stefan-Boltzmann constant ($Wm^{-2}K^{-4}$)

1. Introduction

Silicon Carbide (SiC) is considered an important ceramic material as it is an enabling technology for many applications because of its excellent properties such as its high mechanical stiffness, low density, wide bandgap, low coefficient of expansion, high thermal stability, and resistance to corrosive environments [1]. These applications are high-power microwave devices for commercial and military systems; electronic devices (LED's, MOSFET's); high temperature electronics/optics for automotive, space telescope mirrors in aerospace, laser mirrors and well-logging [2–4]; rugged MEMSs (micro-electro-mechanical sensor) devices for hostile environments; gas and chemical sensors for internal combustion engines, furnaces, and boilers; and solar-blind UV photodetectors [5]. Depending on the application, SiC can be manufactured using many techniques such as extrusion, casting, and die pressing [6–10]. All the mentioned techniques can produce only semi-finished products and post-processing operations such as machining and sintering are needed to produce the final product. But the problem with the post-processing operations is that they are costly operations and can cause many problems such as shrinkage and distortion [11, 12]. Also, producing of complex parts of SiC is a challenge in using these traditional techniques.

Additive manufacturing (AM) can offer the solution for all the previous problems. AM is a manufacturing technique that can be used to produce parts additively layer by layer using the CAD file of the part [13]. AM has many techniques such as powder bed selective laser processing (PBSLP) [14], binder jetting, sheet lamination, and direct energy deposition [15]. PBSLP is an AM technique that can be used to produce parts additively through the deposition and sintering/melting of a powder layer. First, by using certain software, the CAD model of the part that needed to be manufactured is sliced into several layers. Then, a layer of powder with a thickness equal to the thickness of the sliced layer in the model is deposited. At the end, a laser source with certain power and scanning speed is used to scan this layer according to the sliced CAD model. The previous steps are repeated producing the part [16, 17]. PBSLP of ceramic materials can be used to produce dense parts with the same properties of the bulk material with accurate dimensions without any need for post-processing operations to reach the final product [18].

However, the application of this technique in ceramics is facing many problems. The most important problems are high melting/sintering point of ceramic materials and low thermal conductivity [19–22]. The high melting/sintering point of ceramic materials with the sudden increase in the temperature (in order of 10μ seconds) causes high thermal shock to the material [23, 24]. The low thermal conductivity of ceramic materials makes the heat generated by the laser heat source to be kept inside the material and prevent it to be diffused away. As a result, nonhomogeneous heating and cracks are developed [18, 25]. Suocheng *et al* [26] studied the performance improvement of SiC/Si composites manufactured by the combination of PBSLP/Combining reaction-bonded (RB) processes. Subrata and Partha [27] investigated the developed cracks in SiC particulate manufactured by PBSLP to be used in aluminium based metal matrix composite. Hon and Gill [28] applied the PBSLP techniques to produce SiC particulates to be used in composite material. Xiong *et al* [29] studied the effects of using dual binders on the accuracy, microstructure and mechanical properties of SiC particulates used in composites. Nelson *et al* [30] investigated the PBSLP of SiC powders coated with polymer. Hua *et al* [31] studied the addition of silicon effect on the microstructure, mechanical and thermal properties of Carbon fiber reinforced silicon carbide composite (C_f/SiC) manufactured by PBSLP. Laizhen *et al* [32] studied the cracks developed in SiC particulates produced by PBSLP to be used in metal matrix composites. Xiong *et al* [33] studied effects of binders on the dimensional accuracy and mechanical properties of SiC particulates used in composite materials manufactured by PBSLP. Meyers *et al* [34] manufactured SiC parts using PBSLP process. Also, many previous studies [35–38] focused on indirect PBSLP of SiC and other ceramic materials.

From the above literature review, there is a real need to study the PBSLP of SiC as all previous studies focused only on printing SiC particulates to be used for composite materials. Also, PBSLP of SiC is still exhibiting some fatal defects, including low densities and poor mechanical properties. SiC does not have a melt phase under

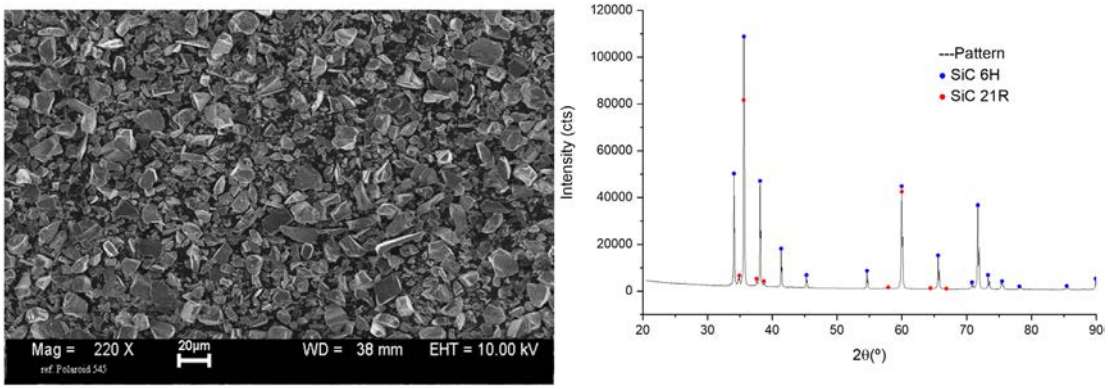

Figure 1. Scanning electron microscopy (SEM) image showing the morphology and XRD pattern (Hexagonal and rhombohedral SiC phases are present) of the Alpha Silicon Carbide powder (Mersen Boostec®).

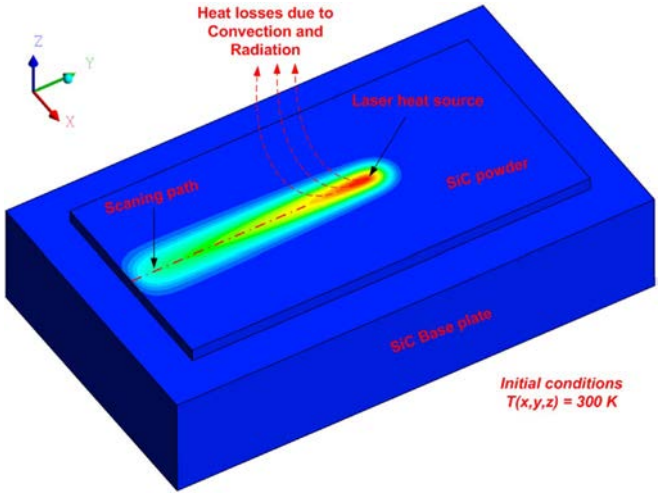

Figure 2. Boundary and initial condition used in the study.

normal atmospheric conditions but instead decomposes at temperatures in excess of 2545 °C into liquid Si and solid C [39]. In consequence, pure selective laser melting of silicon carbide cannot be achieved. This paper, therefore, focuses on the manufacturing of SiC by direct PBSLP and figuring out the effect of the process parameters.

2. Experimental details

2.1. Powder characterization

Alpha-Silicon Carbide powder supplied by Mersen Boostec® with a purity of 98.5 % and $d_{50} = 14\ \mu$m was used in this study. The morphology and the XRD analysis of the powder is shown in figures 1 and 2, respectively. The SEM images shows that the powder did not have a spherical shape (The powder has irregular shape) as it used to be in PBSLP. The irregular shapes of the powder can cause problem in layer depositing due to high developed friction between particles. Therefore, initial testing was carried out and the SiC powder could be deposited as a layer of 25 μm into the powder bed successfully. The XRD indicates that Hexagonal and rhombohedral SiC phases are present in the used powder.

2.2. Laser sintering

PBSLP of SiC was performed on a commercial ORLAS CREATOR 3D printer (250W Yb Fiber laser, laser wavelength = 1070 nm, spot size = 40 μm). Various batches of cubes were scanned to study the effects of PBSLP main process parameters on the sintering and decomposition of SiC. Laser powers (P) of 52 to 235 W and scanning speeds (v) from 300 to 3900 mm s^{-1} were used, while the layer thickness was kept constant at 25 μm and the hatching distance at 40 μm. The laser scanning strategy was a continuous linear pattern and rotated by

Table 1. The thermo physical properties of SiC used in analysis.

Property	Value	References
Density, kg/m^3	3210	Mersen Boostec®
Specific heat	0.0005 T^2 + 1.2911 T + 337.13, (T ⩽ 1273.15)	Mersen Boostec®, [38, 39]
J/kg k	0.0201 T + 1285.9, (1273.15 < T < 2200)	
	1330, (T > 2200)	
	(T, temperature in K)	
Thermal conductivity w/kg k	0.0002 T^2 0.4427 T +295.88, (T ⩽ 1273.15)	
(T, temperature in K)	8E 05 T +5.676, (1273.15 < T < 2200)	
	5.5, (T > 2200)	Mersen Boostec®, [38, 39]
	(T, temperature in K)	
Sintering point, K	>2525	Mersen Boostec®[38, 39]
Latent heat of sintering, J/kg	370000	
Absorptivity	0.55	measured

90 degrees between layers. To prevent oxidation of the powder, an inert argon gas atmosphere was used. The process of PBSLP of SiC in the printer follows the following steps: (i) a layer of SiC powder is deposited on the machine bed by the recoater; (ii) the laser beam starts to scan the layer selectively; (iii) the building bed is lowered by one layer thickness and another layer is deposited above the previously scanned layer. The previous steps are repeated until producing the full part. The building chamber is filled with argon gas.

3. Model development

The transferred heat from the laser source to the powder layer is simulated in the developed model by a user-defined code (UDF) for the laser heat source according to Moser *et al* [40] and the material properties as a function of temperature. The code is compiled and solved using ANSYS Fluent 2020 R1. The Energy equation used to describe the heat transferred from the laser source to the material powder is as follows [40, 41]:

$$\rho C_p \frac{\partial T}{\partial t} = \nabla.(k\ \nabla\ T) + S_h \tag{1}$$

Where T, ρ, C_p and k is the temperature, density, specific heat, and thermal conductivity, respectively. For SiC powder, the material properties such as the thermal conductivity and specific heat are expressed as a function of temperature according to Mersen Boostec®, [38, 39] and showed in table 1 . The heat source S_h in equation (1) is representing the laser source which has a Gaussian profile and can be written as follow [40]:

$$S_h = AI_o\alpha\ \exp\left(-2\frac{(x - v_x t)^2 + (y - v_y t)^2}{\omega^2} - \alpha z\right) \tag{2}$$

Where α is the effective absorption coefficient, A is the material absorptivity, I_o is the laser intensity, ω is the laser characteristic radius, and according to [40]:

$$I_o = \frac{2P}{\pi\ \omega^2} \tag{3}$$

$$\alpha = \frac{1}{D_p} \tag{4}$$

$$\omega = \frac{D_b}{2 \times 2.146} \tag{5}$$

D_b in equations (4) and (5) is the average powder particle diameter. The factor of 2.146 in equation (5) was derived from calculating the distance from the laser centre at which the laser intensity distribution has $I/I_0 = 1/e2$ (0.135). This allow I_0 to be easily and more accurately calculated by using the characteristic radius according to [40]. Initial and boundary conditions used in this analysis are shown in figure 2 and are according to equations (5) and (6) as follows:

$$T(x, y, z)_{t=0} = T_O \tag{6}$$

$$-\mathrm{k}\left(\frac{\partial T}{\partial z}\right) = S_h - h_{cov}(T_a - T_s) - \sigma\varepsilon(T_a^4 - T_s^4) \tag{7}$$

Where T_O is the room temperature and is set to 300 K, h_{cov} is the heat convection coefficient, T_a is the powder layer initial temperature, T_s is the surroundings temperature, ε is the radiation coefficient, and σ is Stefan-Boltzmann constant.

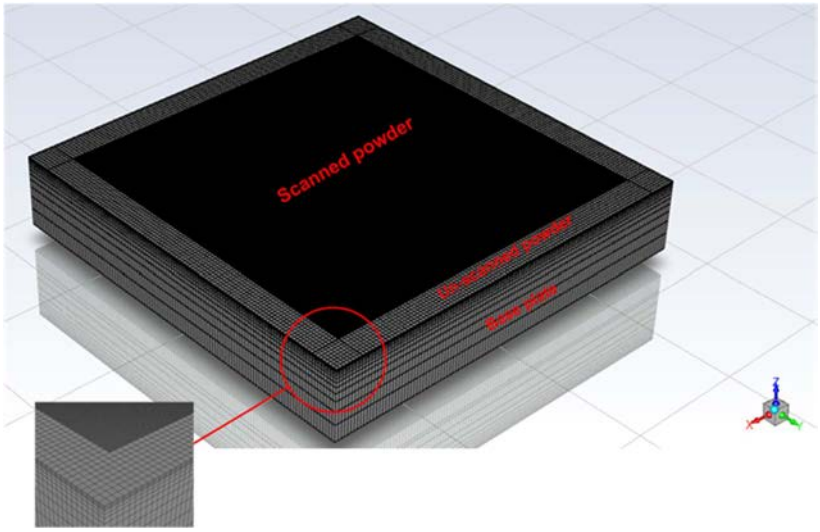

Figure 3. The model geometry and computational domain used in the analysis.

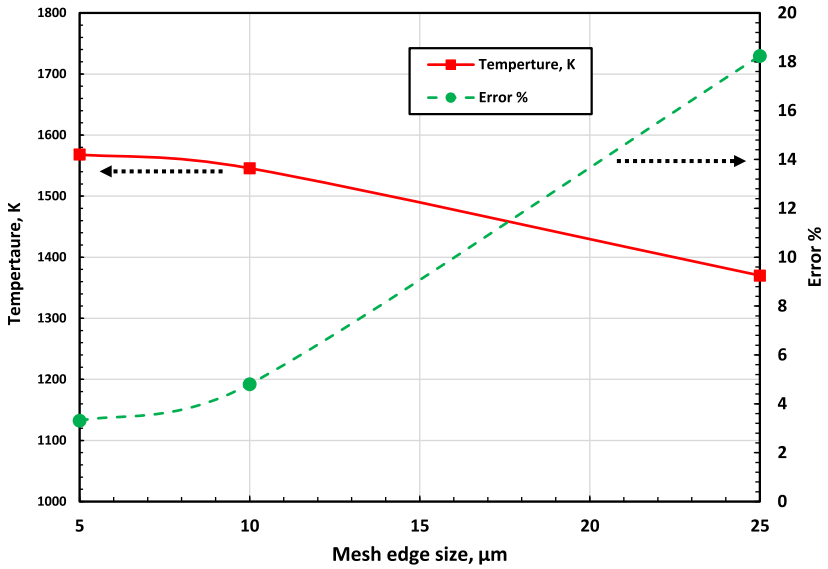

Figure 4. Mesh density analysis.

Table 2. Geometrical model and dimensions.

Parameter	Base plate	Powder layer
Length (mm)	6.4	6
Width (mm)	6.4	6
Thickness (mm)	0.5	0.025

Also, the melting and solidification module available in Ansys Fluent [41] was used to calculate the sintering region happened during the scanning process.

4. Numerical methodology

In this section, a description of the physical geometry and the computational domain used in the analysis is presented followed by a description for the numerical solution procedure of the governing equations. The validation of the obtained results with experimental results is also provided.

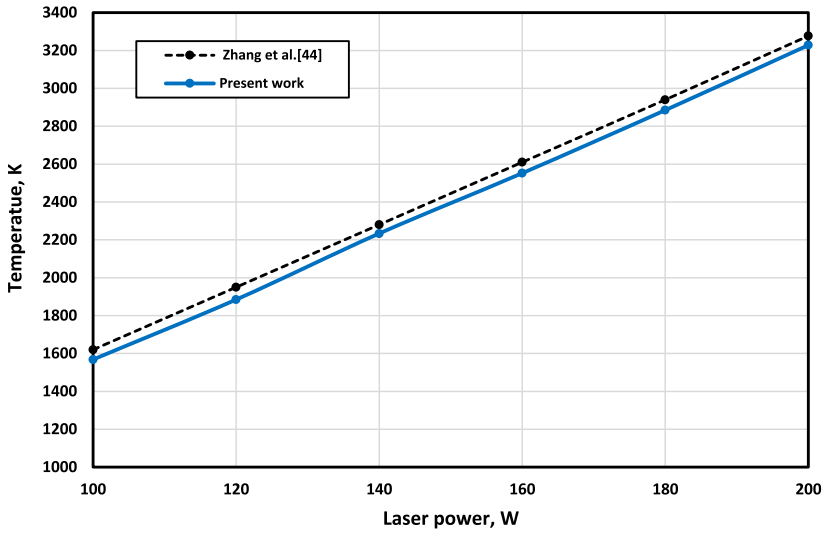

Figure 5. Validation of the developed model results with Zhang *et al* [39] and mesh density analysis.

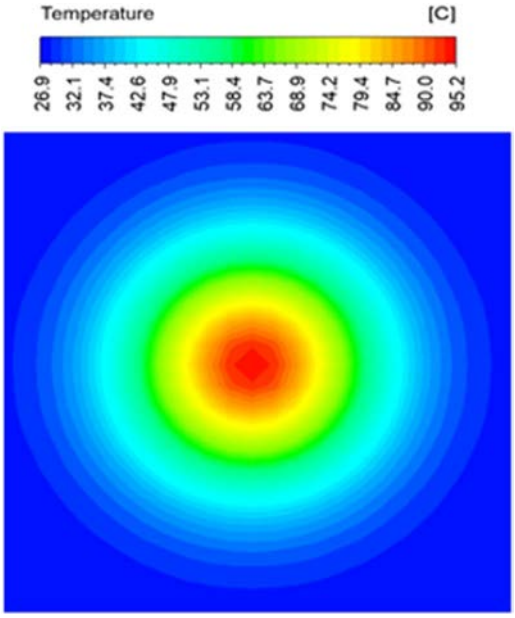

Figure 6. Temperature contour obtained by the numerical model using conditions close to those used in the studies reported in [35] and [40].

4.1. Model geometry and the computational domain

The model geometry and the computational domain (mesh) used in the analysis is shown in figure 3. The model consists of three parts: the base plate, the scanned powder, and the un-scanned powder. The un-scanned powder is concluded in the model to take into consideration the heat transferred to it. The dimensions of the model are summarized in table 2.

4.2. Model validation and mesh density analysis

The CFD model was solved using ANSYS FLUENT 2020 R1 in a transient mode. Thee time step size and number of iterations per time step used in the numerical solution were selected and tested to give more fine results without any effects on the obtained temperature and contours of sintering pool. The timestep size used in this study was 0.00001 s and the iterations per time step was 20. Also, all measurements were performed when the laser beam temperature become stable (no change in the temperature with the scanning time). Three different mesh edge sizes (25 μm, 10 μm and 5 μm) were used in the mesh density analysis where the obtained temperature from each mesh edge size is showed in figure 4. The results showed there is a big difference in the calculated temperature between the mesh edge size 25 μm and 10 μm. Reducing the mesh edge size from 10 μm

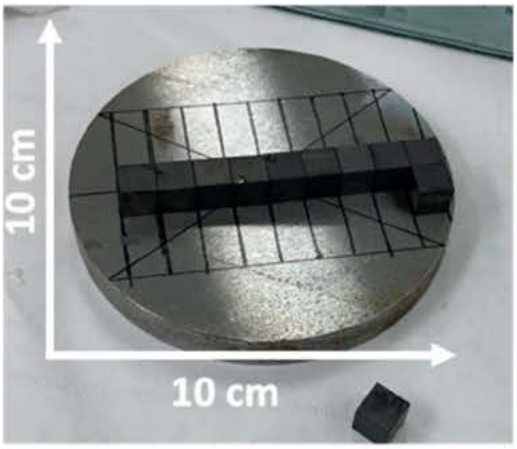

Figure 7. SiC cubes glued onto the 3D printer support.

Table 3. The laser powers and scanning speeds used in this study. Grey used / White not used.

Scanning speed mm/s	Laser power (W)						
	52	76	107	139	171	203	235
3900							
3300							
3000							
2700							
2500							
2100							
2000							
1500							
1000							
900							
300							

to 5 μm, gave a small difference between the calculated temperature. Regarding the error percentage with the experimental results, the mesh size 5 μm gave about 3.3 % which is considered acceptable. Therefore, the mesh edge size 5 μm was used in this study as it gave a very close result and to reduce the solving time.

The obtained results using the mesh edge size 5 μm were compared with the available data from Zhang *et al* [42] as shown in figure 5. The comparison showed that there is a good agreement between the two results. The maximum error between them was 3.34%. Another validation was carried out for the confirmation of model validation. The temperature contour as shown in figure 6 obtained by the numerical model using conditions close to those used in the studies reported in [40, 43] and the contour captured using a thermal camera as shown in figure 7(c) of [40, 43] confirms a good agreement with a calculation error of 1.24 %.

5. Results and discussion

5.1. Experimental results

To assure the additive manufacturing of the samples, good sintering conditions must be reached since there is no binder or liquid phases to join the powder particles together. In these terms, first built layers are crucial. To assure this important fact, SiC cubes (10 × 10 × 10 mm) were glued onto the baseplate 3D printer, as can be seen in figure 7, to avoid the metal and SiC interaction and ensure the sintering and construction of the first layers. Moreover, the addition of small cubes as new supports, facilitates the recuperation and characterization of the manufactured samples. Different laser power values (ranging from 52W to 235W) and scanning speed values (ranging from 300 to 3900 mm s^{-1}) were used to PBSLP of SiC as summarized in table 3. These parameters were chosen because they are the maximum and minimum value allowed for laser power and scanning speed by the 3D printer used. The objective is to test experimentally the entire range of parameters to find the range of values

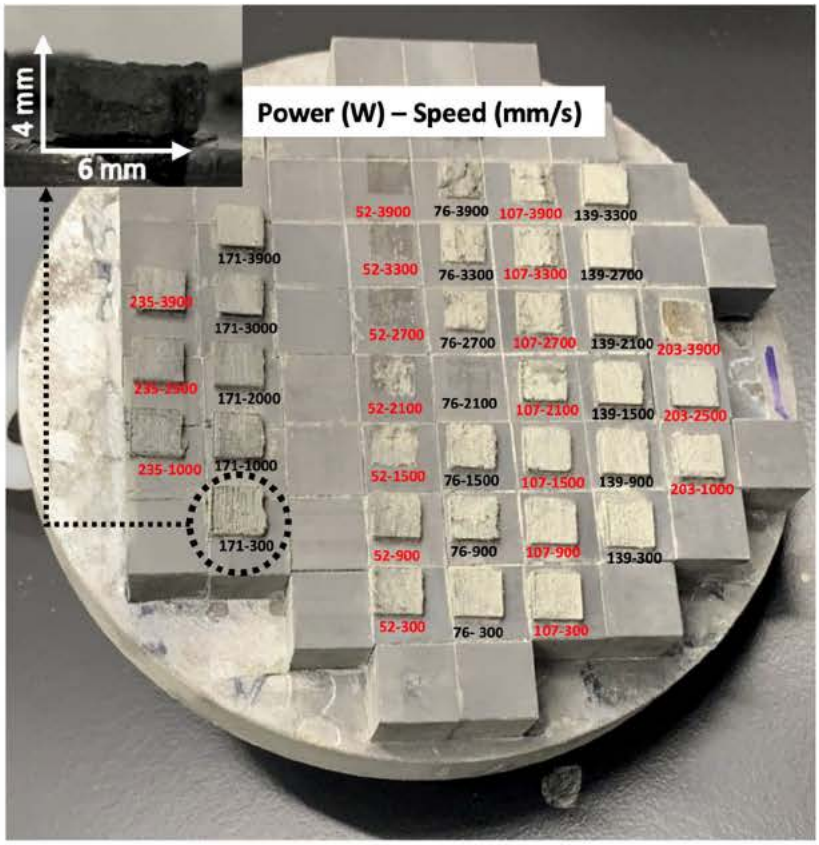

Figure 8. PBSLP of SiC samples onto the SiC cubes using different laser powers and scanning speeds as written on each sample.

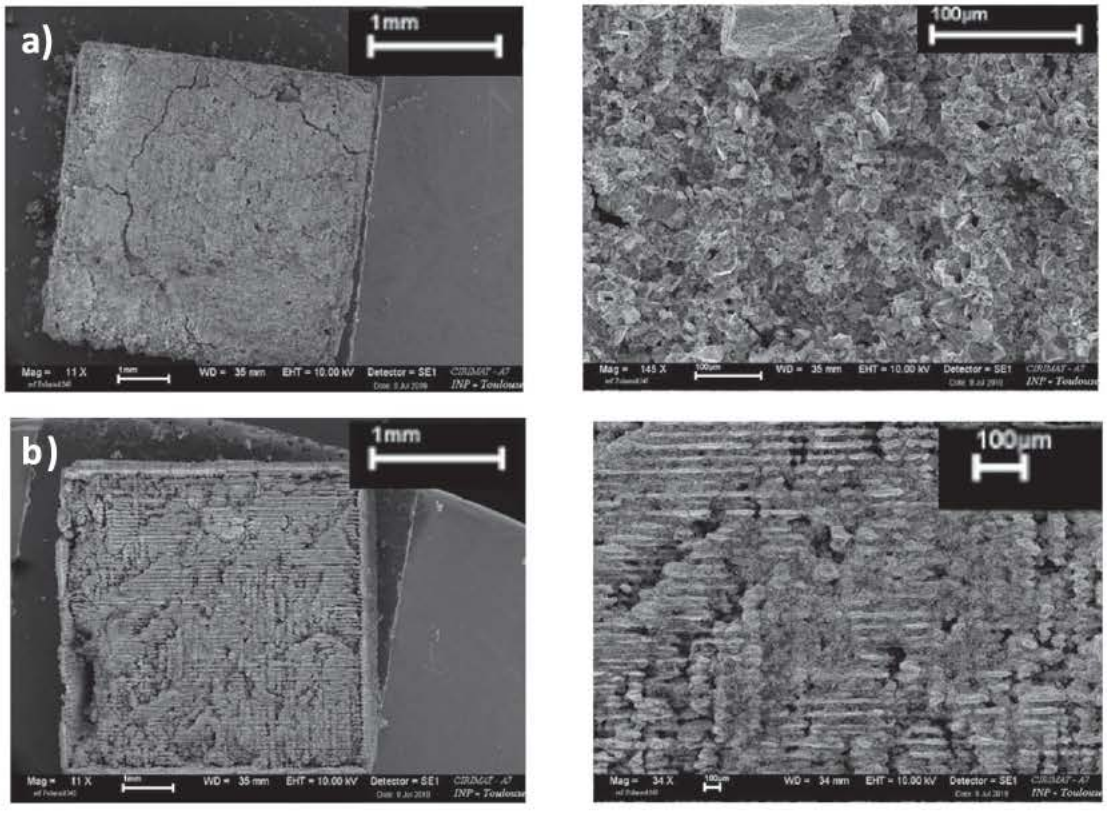

Figure 9. (a) Manufactured SiC exhibits partial sintering (52 W 900 mm s ^{1}) and (b) manufactured SiC exhibits decomposition (76 W 300 mm s ^{1}): low (left) and high (right) magnification.

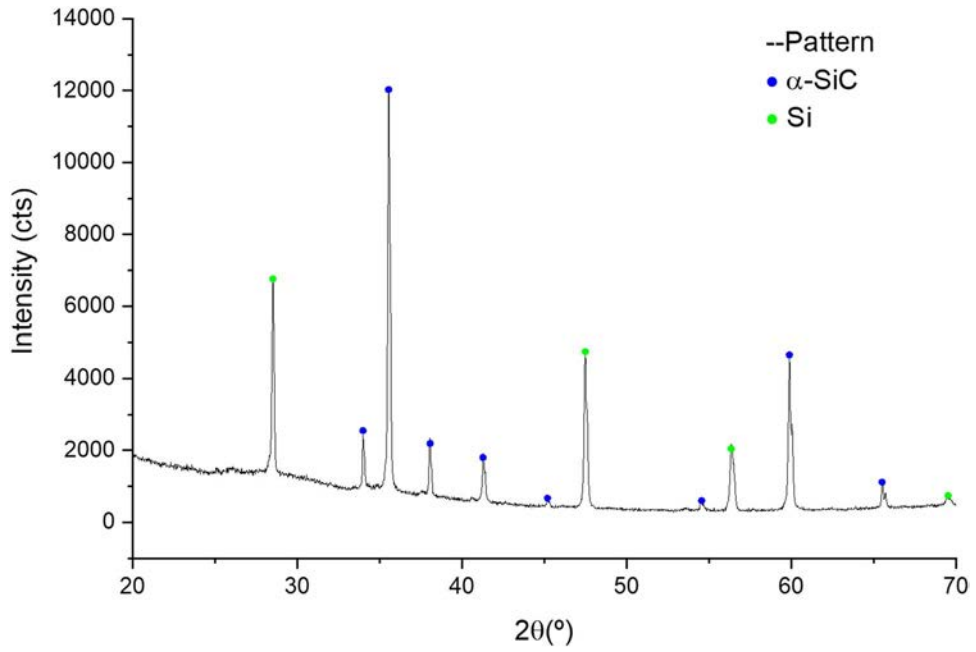

Figure 10. XRD spectra of the 76 W and 300 mm s ^{1} SiC manufactured part.

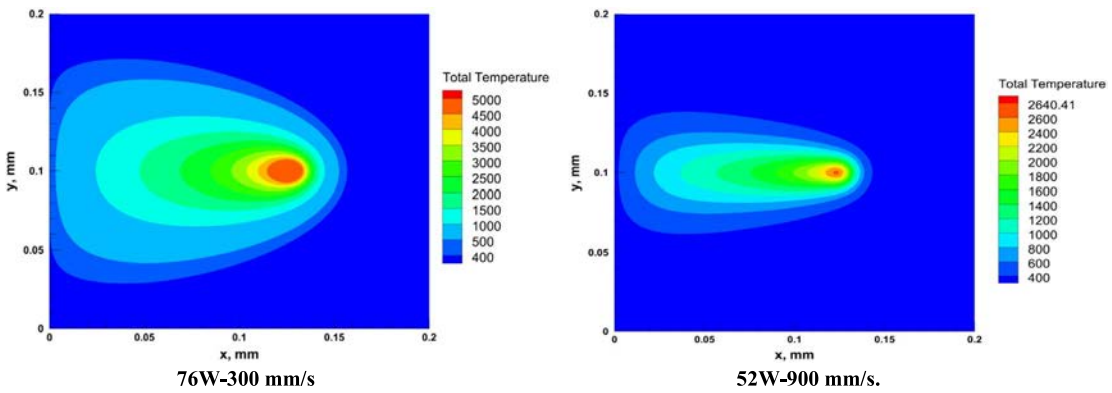

Figure 11. Laser spot temperature contour for the 76 W 300 mm s ^{1} and 52 W 900 mm s ^{1} samples.

for which the PBSLP of SiC is possible in accordance to the simulation results. The obtained results are showed in figure 8. These SiC samples manufactured by PBSLP failed either due to very fast scanning speed or very high laser power, which leads to full SiC decomposition. There are two samples, using 52W with 900 mm s ^{1} and 76W with 300 mm s ^{1}, that succeeded to PBSLP of SiC but with defects. These two samples were analysed using SEM (figure 9) to determine the sintering and/or decomposition during the process.

The results showed that only two samples exhibit different structure of the top surface. The sample manufactured using 52 W-900 mm s ^{1} shows clusters of particles as can be seen in figure 9(a). The sample manufactured using 76 W-300 mm s ^{1} shows, in figure 9(b), a characteristic pattern with needle-like protrusions in tracks parallel to the scanning directions of the laser. This originated from the hatch distance and the scanning strategy (linear with 90° degrees rotation between each layers).

For the sintering/decomposition state, the sample manufactured using 52 W-900 mm s ^{1} showed partial sintering and no melting was observed as can be seen in figure 9(a). On the other hand, in figure 9(b), using 76 W-300 mm s ^{1}, melted regions can be observed, probably originated by the SiC decomposition, resulting in resolidified silicon. To interpret the melted regions of the SiC manufactured samples, since SiC has not a liquid phase, XRD spectra of the 76 W-300 mm s ^{1} sample is shown in Figure 10. The phases present in the SiC manufactured sample are silicon carbide and silicon, therefore, since initially just Alpha-SiC was supplied to the printer, these melted regions are resulting from a beginning of SiC decomposition leading to α-SiC and Si (with CO_2 release). By contrast, Si was not observed by XRD for the 52 W-900 mm s ^{1} sample.

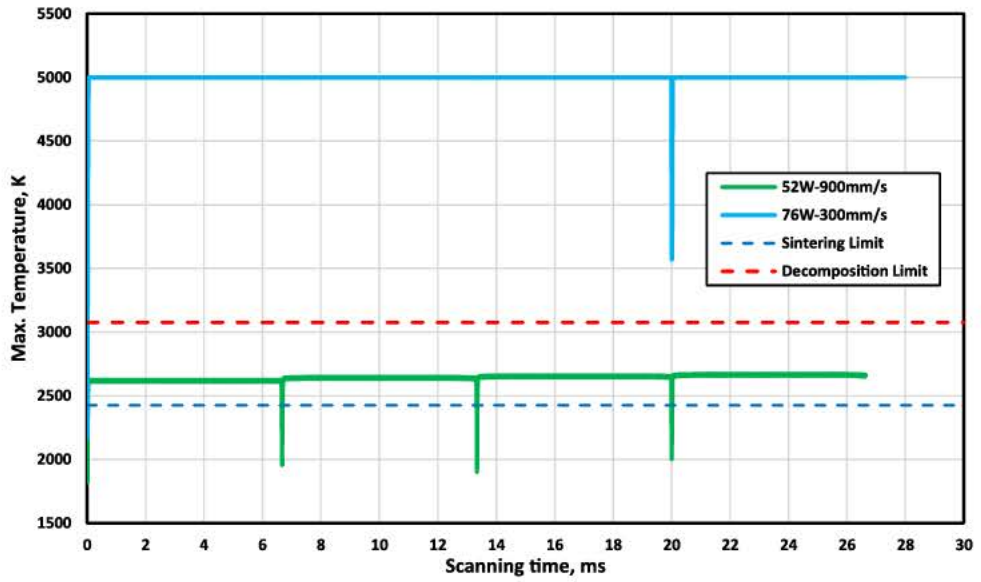

Figure 12. Temperature history for 76 W 300 mm s ^{1} and 52 W 900 mm s ^{1}.

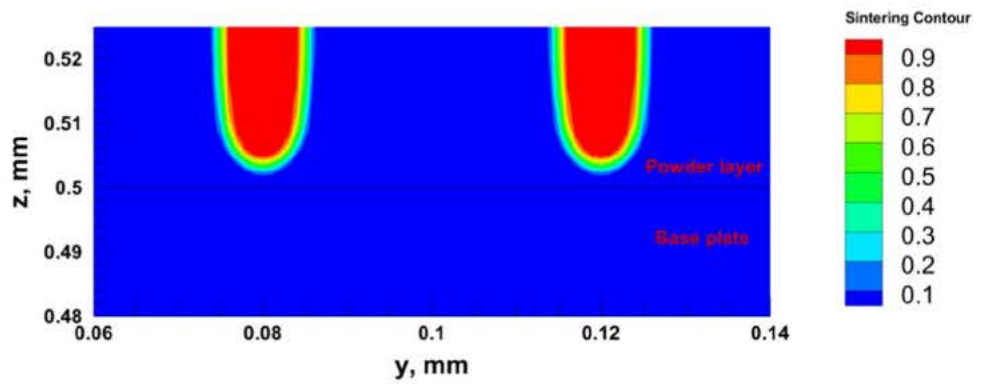

Figure 13. Sintering region for two adjacent paths for the 52 W 900 mm s ^{1} sample.

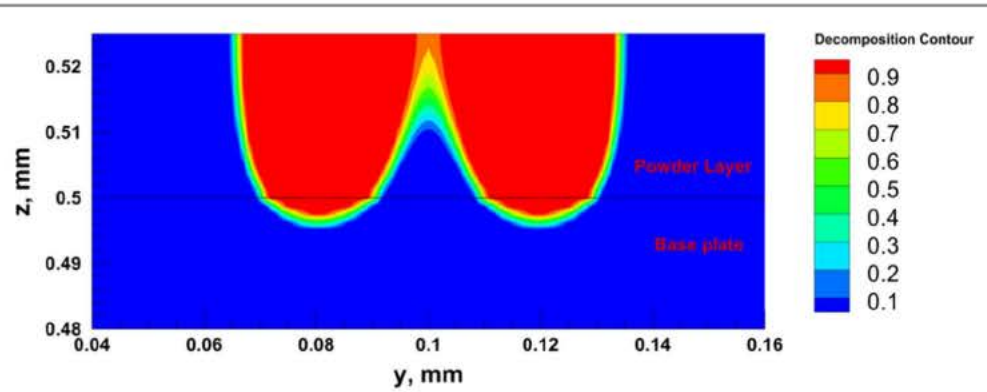

Figure 14. Sintering region for two adjacent paths for the 76 W 300 mm s ^{1} sample.

5.2. Numerical results

The numerical model was used to analyse the PBSLP of one deposited layer for the 76 W-300 mm s ^{1} and 52 W-900 mm s ^{1} cases to deeply understand and see what happened during the scanning process. Also, to clearly illustrate the results from the experimental study. Figure 11 shows the temperature contour of the laser spot for 76 W-300 mm s ^{1} and 52 W-900 mm s ^{1}. The case 76 W-300 mm s ^{1} gives high temperature distribution values compared to the case 52 W-900 mm s ^{1} due high power and low scanning speed used. The maximum

temperature reaches 5000 K (This value is based on numerical calculations and cannot be obtained in reality as the material will be evaporated before reaching this value) for the case 76 W-300 mm s ^{1} at the laser spot centre, which means that all powder located in this region will be totally decomposed and evaporated. The case of 52 W-900 mm s ^{1} gives a maximum temperature of 2606 K at the laser spot centre, which is above the sintering limit of SiC. So, this condition is more promising than the case of the 76 W-300 mm s ^{1} sample.

Figure 12 shows the history for the maximum temperature of laser spot centre during scanning process for both cases. The time that the case 52 W-900 mm s ^{1} consumed to finish 3 paths, the 76 W-300 mm s ^{1} sample finished only 1 path. For the case 52 W-900 mm s ^{1}, the temperature history lied between the sintering and the decomposition limits so that sintering happened without decomposition, as revealed in the SEM analysis showed in figure 9(a). However, as can be seen in figure 9(a), a partial sintering is observed but there are also un-sintered powder. This can be interpreted by figures 13 and 14 that show the sintering region for two adjacent paths using the conditions 52 W-900 mm s ^{1} and 76 W-300 mm s ^{1}, respectively. Figure 13 shows that there are un-sintered powders between the adjacent paths, and this mainly caused the partial sintering shown in figure 9(a). This problem can be solved by optimizing the hatching distance. Also, figure 13 shows that the laser beam was not able to sinter the whole layer thickness so that lower layer thickness values are recommended.

For the case 76 W-300 mm s ^{1}, figure 12 shows that the temperature history is high above the decomposition limit leading effectively to the partial decomposition of SiC and the formation of elemental Si as supported by XRD analysis (figure 10). Figure 14 shows the decomposition region of two adjacent paths for the case 76 W-300 mm s ^{1}, where the powder located in the path of the laser beam will be decomposed and formed the grooves showed in the SEM analysis in figure 9(b). Also, there is a partially sintered region between adjacent paths as showed in figure 14, which explains the peak formation in the parallel tracks showed in the SEM analysis in figure 9(b). By measuring the average width of the grooves showed in the SEM image in figure 9(b), an experimental value of approximately 40 μm is found while it is 36.5 μm in figure 14 (numerical value) with 8.5% percentage error. The good agreement in the experimental/modelling coupling approach proves the ability of the developed model to effectively and accurately simulated the PBSLP process.

6. Conclusions and future study

The PBSLP of SiC was studied experimentally and numerically. The PBSLP was performed on a commercial ORLAS CREATOR 3D printer. The laser powers used ranged from 52 to 235 W and the scanning speeds ranged from 300 to 3900 mm s ^{1} were used. The layer thickness was kept constant at 25 μm and the hatching distance at 40 μm. The following points are concluded from this study:

1. The PBSLP of SiC is highly possible with the optimization of the process parameters.
2. Many values of laser power and scanning speed were used to study the PBSLP of SiC and only the conditions 52W-300 mm s ^{1} and 76W-900 mm s ^{1} have been successful to manufacture SiC with however defects.
3. Using the case 52W-300 mm s ^{1}, there was un-sintered region found in the SEM analysis. When the developed numerical model used to analyse this condition, it was found that the input heat was not able to sinter the powder between the adjacent paths and the whole depth of the powder layer. This is mainly due to the hatching distance and the layer thickness used. These parameters have to be study and optimize for successful PBSLP of SiC.
4. Under the condition 76W-900 mm s ^{1}, the manufactured SiC exhibited more defects due to the high input heat to the powder, which produces tracks (peaks and grooves) on the surface of the printed layer.
5. A more precise guide for the selection of the laser power and the scanning speed for PBSLP of SiC is still necessary.
6. The developed numerical model proved its ability to be effectively used in the optimization of the process parameters for successful PBSLP of SiC.

For future study, the developed numerical model is going to be used to optimize the layer thickness and the hatching distance for successful PBSLP of SiC. Also, a guide for the selection of the laser power and the scanning speed currently in progress should be achieved. Also, the effect of the process parameters on the quality of SiC samples will be analyzed in the coming study.

Acknowledgments

This project, DOC-3D-printing, has received funding from the European Union's Framework Program for Research and Innovation Horizon 2020 (2014–2020) under the Marie Skłodowska-Curie Grant Agreement No. [764935].

Data availability statement

The data that support the findings of this study are available upon reasonable request from the authors.

ORCID iDs

Alejandro Montón https://orcid.org/0000-0003-3948-9520
Mohammed Abdelmoula https://orcid.org/0000-0002-7343-6863
Gökhan Küçüktürk https://orcid.org/0000-0002-2978-8968
Francis Maury https://orcid.org/0000-0003-2796-9738
David Grossin https://orcid.org/0000-0002-4320-2919

References

[1] Kimoto T and Cooper J A 2014 Physical Properties of Silicon Carbide *Fundamentals of Silicon Carbide Technology* ed T Kimoto and J Cooper A (Singapore: Wiley Singapore Pte. Ltd) pp 11 38
[2] Renotte E *et al* 2019 Full SiC derotator optics for METimage: preliminary design and verification approach *en Int. Conf. on Space Optics ICSO 2018 (Chania, Greece)* p 303
[3] Bougoin M, Mallet F, Lavenac J, Gerbert Gaillard A, Ballhause D and Chaumeil Y F 2019 Full SiC EUCLID's very large telescope *en Int. Conf. on Space Optics ICSO 2018 (Chania, Greece)* p 60
[4] Leray C *et al* 2017 Design and proof of concept of an innovative very high temperature ceramic solar absorber *AIP Conf. Proc.*030032
[5] Kimoto T and Cooper Y J A 2014 *Fundamentals of Silicon Carbide Technology: Growth, Characterization, Devices and Applications* (New York: Wiley)
[6] Tweed J H 1991 Manufacture of 2014 aluminium reinforced with SiC particulate by vacuum hot pressing *Mater. Sci. Eng. A* 135 73 6
[7] Song M and He Y Y H 2010 Effects of die pressing pressure and extrusion on the microstructures and mechanical properties of SiC reinforced pure aluminum composites *Mater. Des.* 31 985 9
[8] Poorteman M, Descamps P, Cambier F, Leriche A and Thierry Y B 1993 Hot isostatic pressing of SiC platelets/Y TZP composites *J. Eur. Ceram. Soc.* 12 103 9
[9] Wang Z, Song M, Sun C, Xiao D and He Y Y 2010 Effect of extrusion and particle volume fraction on the mechanical properties of SiC reinforced Al Cu alloy composites *Mater. Sci. Eng., A* 527 6537 42
[10] Nie K B, Wang X J, Xu L, Wu K, Hu X S and Zheng Y M Y 2012 Effect of hot extrusion on microstructures and mechanical properties of SiC nanoparticles reinforced magnesium matrix composite *J. Alloys Compd.* 512 355 60
[11] Ozer I O, Suvaci E, Karademir B, Missiaen J M, Carry C P and Bouvard Y D 2006 Anisotropic sintering shrinkage in alumina ceramics containing oriented platelets *J. Am. Ceram. Soc.* 89 1972 6
[12] Huang H and Liu Y Y C 2003 Experimental investigations of machining characteristics and removal mechanisms of advanced ceramics in high speed deep grinding *Int. J. Mach. Tools Manuf* 43 811 23
[13] Gibson I, Rosen D W and Stucker Y B 2014 *Additive Manufacturing Technologies* 17 (Berlin: Springer)
[14] Grossin D *et al* 2021 A review of additive manufacturing of ceramics by powder bed selective laser processing (sintering/melting): Calcium Phosphate, Silicon Carbide, Zirconia, Alumina, and their composites *Open Ceramics* 5 100073
[15] Adekanye S A, Mahamood R M, Akinlabi E T and Owolabi Y M G 2017 Additive manufacturing: the future of manufacturing: Dodajalna (3D) Tehnologija: Prihodnost Proizvajanja *Materiali in Tehnologije* 51 709 15
[16] Kruth J P, Froyen L, Van Vaerenbergh J, Mercelis P, Rombouts M and Lauwers Y B 2004 Selective laser melting of iron based powder *J. Mater. Process. Technol.* 149 616 22
[17] Rombouts M, Kruth J P, Froyen L and Mercelis Y P 2006 Fundamentals of selective laser melting of alloyed steel powders *CIRP Annals Manufacturing Technology* 55 187 92
[18] Sing S L *et al* 2017 Direct selective laser sintering and melting of ceramics: a review *Rapid Prototyping Journal* 23 611 23
[19] Yves Christian H, Jan W, Wilhelm M, Konrad W and Reinhart Y P 2010 Net shaped high performance oxide ceramic parts by selective laser melting *Phys. Proc.* 5 587 94
[20] Wilkes J, Hagedorn Y C, Meiners W and Wissenbach Y K 2013 Additive manufacturing of ZrO_2 Al_2O_3 ceramic components by selective laser melting *Rapid Prototyping Journal* 19 51 7
[21] Liu Q, Danlos Y, Song B, Zhang B, Yin S and Liao Y H 2015 Effect of high temperature preheating on the selective laser melting of yttria stabilized zirconia ceramic *J. Mater. Process. Technol.* 222 61 74
[22] Khmyrov R S, Protasov C E, Grigoriev S N and Gusarov Y A V 2016 Crack free selective laser melting of silica glass: single beads and monolayers on the substrate of the same material *International Journal of Advanced Manufacturing Technology* 85 1461 9
[23] Zheng Y, Zhang K, Liu T T, Liao W H, Zhang C D and Shao Y H 2019 Cracks of alumina ceramics by selective laser melting *Ceram. Int.* 45 175 84
[24] Juste E, Petit F, Lardot V and Cambier Y F 2014 Shaping of ceramic parts by selective laser melting of powder bed *J. Mater. Res.* 29 2086 94
[25] Gan M X and Wong Y C H 2017 Properties of selective laser melted spodumene glass ceramic *J. Eur. Ceram. Soc.* 37 4147 54
[26] Song S, Gao Z, Lu B, Bao C, Zheng B and Wang Y L 2020 Performance optimization of complicated structural SiC/Si composite ceramics prepared by selective laser sintering *Ceram. Int.* 46 568 75

[27] Ghosh S K and Saha Y P 2011 Crack and wear behavior of SiC particulate reinforced aluminium based metal matrix composite fabricated by direct metal laser sintering process *Mater. Des.* **32** 139 45
[28] Hon K K B and Gill Y T J 2003 Selective laser sintering of SiC/polyamide composites *CIRP Annals Manufacturing Technology* **52** 173 6
[29] Xiong B W *et al* 2013 Study on dual binders for fabricating SiC particulate preforms using selective laser sintering *Composites Part B: Engineering* **48** 129 33
[30] Christian Nelson J, Vail N K, Barlow J W, Beaman J J, Bourell D L and Marcus Y H L 1995 Selective laser sintering of polymer coated silicon carbide powders *Ind. Eng. Chem. Res.* **34** 1641 51
[31] Fu H *et al* 2019 Effect of silicon addition on the microstructure, mechanical and thermal properties of Cf/SiC composite prepared via selective laser sintering *J. Alloys Compd.* **792** 1045 53
[32] Jin L, Zhang K, Xu T, Zeng T and Cheng Y S 2018 The fabrication and mechanical properties of SiC/SiC composites prepared by SLS combined with PIP *Ceram. Int.* **44** 20992 9
[33] Xiong H *et al* 2013 Effects of binders on dimensional accuracy and mechanical properties of SiC particulates preforms fabricated by selective laser sintering *Composites Part B: Engineering* **44** 480 3
[34] Meyers S, Kruth J and Vleugels J 2015 Direct selective laser sintering of reaction bonded silicon *Materials Science* 1750 8
[35] Chen A N *et al* 2019 Enhancement mechanism of mechanical performance of highly porous mullite ceramics with bimodal pore structures prepared by selective laser sintering *J. Alloys Compd.* **776** 486 94
[36] Chen A N *et al* 2018 High porosity mullite ceramic foams prepared by selective laser sintering using fly ash hollow spheres as raw materials *J. Eur. Ceram. Soc.* **38** 4553 9
[37] Parmar K and Negi Y N S 2017 Tailoring structural and electrical properties of A site non stoichiometric $Na_{0.5}$ $Bi_{0.5}$ TiO_3 ceramic at different sintering temperature *Advances in Applied Ceramics* **116** 8 18
[38] Xiao Q D, Zhou F and Wu Y S 2017 Ti_3 SiC_2 friction material prepared by novel method of infiltration sintering *Advances in Applied Ceramics* **116** 2 7
[39] Silva A M R R 2019 *Additive Manufacturing of Technical Ceramics* Escola Superior de Tecnologia e Gestão, Instituto politecnico de Leiria Master degree in Product Design EngineeringAdditive Manufacturing of Technical Ceramics (http://hdl.handle.net/10400.8/4021)
[40] Moser D, Beaman J and Fish Y S 2016 Multi layer computational modeling of selective laser sintering processes *Proc. of the ASME 2014 Int. Mechanical Engineering Congress and Exposition IMECE2014* pp 1 11
[41] ANSYS Inc. 2013 *ANSYS Fluent Theory Guide* 373 464 Release 18.2, 15317, n.o November 2013, pp 373 464
[42] Zhang K, Liu T, Liao W, Zhang C, Zheng Y and Shao Y H 2018 Simulation of the thermal behavior and analysis of solidification process during selective laser melting of alumina *2018 Annual International Solid Freeform Fabrication Symposium An Additive Manufacturing Conference (Austin, Texas, USA, 13 15 August 2018)* 1808 20 (http://utw10945.utweb.utexas.edu/sites/default/files/2018/149%20SimulationoftheThermalBehaviorandAnalysisof.pdf)
[43] Edith Wiria F, Fai Leong K and Kai Chua Y C 2010 Modeling of powder particle heat transfer process in selective laser sintering for fabricating tissue engineering scaffolds *Rapid Prototyping Journal* **16** 400 10